7.0 QUANTITATIVE DETERMINATION OF ZINC COORDINATION BY CS-XAS

X-ray absorption spectroscopy is a powerful tool that can be used to examine the coordination environment of the selected element in complex matrices. Although EXAFS has been used primarily in the past for the study of concentrated samples such as alloys and other pure compounds, the development of second and third-generation synchrotron sources has provided the flux of X-ray photons required for environmental analysis. Much of the previous environmental XAS studies have focused on examining contaminants on extremely well defined surfaces, such as synthetic iron oxides or well defined clay particles (Fendorf *et. al.*, 1997; Manning *et. al.*, 1998; Strawn and Sparks, 1999). However, it is unlikely that the environment is truly composed of such simple systems. The XAS work presented here uses quadratic-linear programming to perform spectral decomposition in order to characterize sediments through a library of standard compounds used as a basis set. To validate this technique, comparisons were made to sediments characterized through wet chemical sequential extractions.

As was seen in the previous chapter, zinc is present in several different chemical and morphological forms at different locations in the lake. XAS was used to establish chemical profiles of zinc in the sediments of the lake at each of the sampling sites. Both qualitative and quantitative measurements have been carried out. These profiles show that zinc exists in many varied coordination environments throughout Lake DePue. In general, these profiles show that as the concentration of zinc in the sediments decreases,

the dominant form of zinc changes from labile forms, such as carbonates and aqueous-like coordinations, to sulfide coordinations.

7.1 SEDIMENT EXAFS PROFILES

Spectra with experimental error bars for a typical sample from Lake DePue sediment are shown in Figure 7.1. Samples were examined from cores at a resolution of approximately one to five centimeters. Resolution was the finest at the sediment water interface, and the largest at depth. These cores were taken from the lake in September of 1998 and represent samples from the major sedimentary regions of the lake. Cores were examined from other seasons, from July 1998 through August 2000, and showed similar general results of speciation trends for each of the sedimentary environments. Figure 7.1 shows the spectra and the associated error at each step in the data analysis procedure (normalized μ, unfiltered $k^3 \chi(k)$, and radial distribution function (RDF) uncorrected for phase shift). The error bars at each point reflect the actual statistics of the EXAFS measurements and the respective propagation of the error as explained in Chapter 6. The calculated fits to the dataset are also represented in Figure 7.1 as the solid lines. In nearly all instances, the fit is within the limits of the error bars. More importantly, the fit captures all of the significant features and trends in the data. Figure 7.2 shows the raw unfiltered EXAFS spectrum of the sediment sample and all of the individual components that were used to decompose the spectrum. In this sample, the major species of Zn present included $Zn_3CO_3(OH)_4$, ZnS, $Zn_3(PO_4)_2$, hydrated Zn, and Zn

associated with iron oxides. The amplitude of each of the standard components is shown proportional to its respective contribution to the total amount calculated in the fit of the sample.

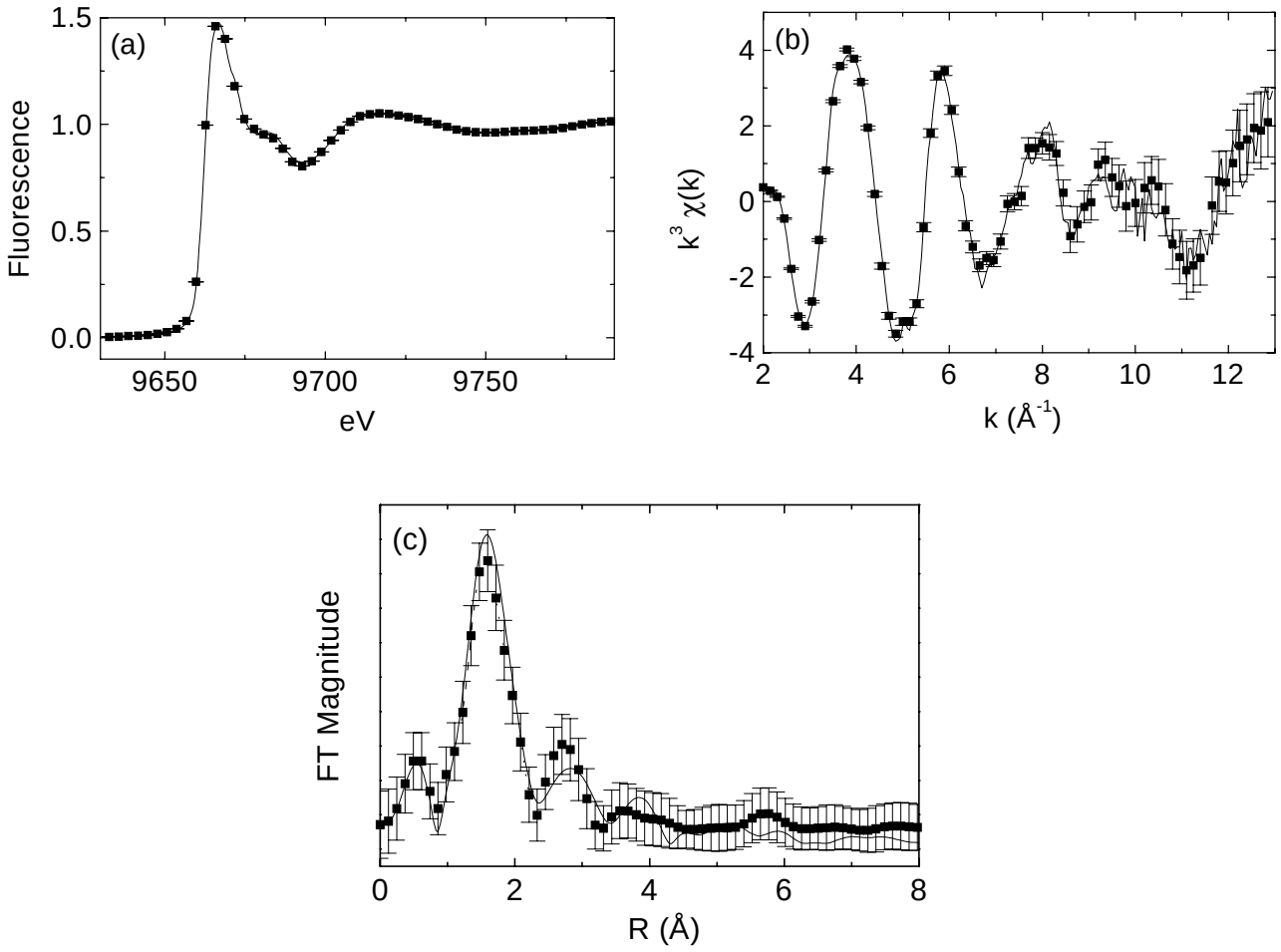

Figure 7.1: EXAFS spectra of Lake DePue samples. In each graph, the data and their associated error bar is shown with every fourth point plotted to allow clear representation of the spectrum. The solid line is the calculated fit to the data. (a) Normalized data in the near-edge region. (b) k^3-weighted EXAFS data. (c) Pseudo-radial distribution function (RDF). Note that data are not corrected for phase shift, thus radial distances do not reflect true bond lengths.

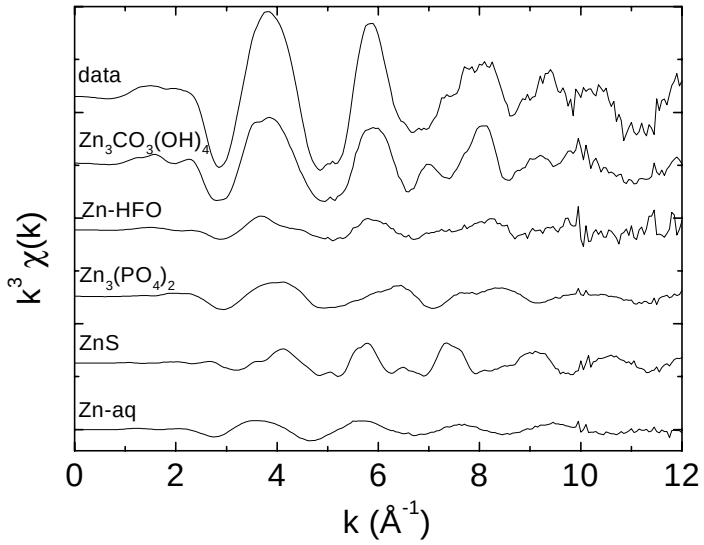

Figure 7.2: EXAFS spectrum of Lake DePue sediment from location C1. Upper spectrum is the actual data set collected. Stacked EXAFS below show the individual weighted contribution of each fitted component to the original spectrum.

Figure 7.3 shows the differences in the EXAFS spectra and RDFs as a function of depth in the sediment. Sediments were collected from site C1. As the speciation of Zn changes as a function of depth in the sediments, small transitions can be seen in the k^3-weighted EXAFS. These changes are more clearly seen in the Fourier transform of the spectra, which gives an average pseudo-radial distribution function (RDF) (uncorrected for phase-shift) of atoms around the X-ray absorber, in this case zinc. These RDFs are shown in Figure 7.3b. These show a distinct shift toward longer bond lengths in the first coordination shell of zinc at greater sediment depth. This is due to a change in the coordination of Zn from primarily Zn-O to Zn-S. EXAFS of the standards showed that the Zn-O bond length is typically represented in the phase uncorrected RDF by 1.53-1.56

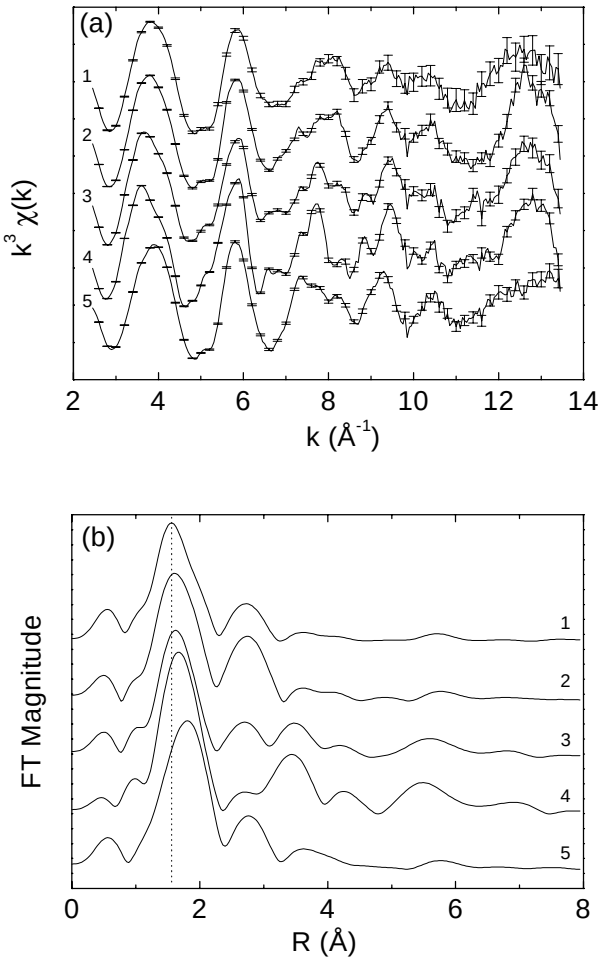

Figure 7.3: Stacked sediment depth profiles of (a) EXAFS signal and (b) RDFs from location C1. The EXAFS plot shows the error associated with every four points in the spectrum for clarity. Depth legend: (1) = 0 cm; (2) = 3 cm; (3) = 8 cm; (4) = 15 cm (5) = 20 cm.

Å in carbonates and phosphates (actual bond lengths 2.0-2.1 Å (Wyckoff, 1960)), whereas the Zn-S bond length is represented by 1.94 Å (actual bond length 2.34 Å (Wyckoff, 1960)). This shift in zinc coordination is exemplified in Figure 7.4 where the transition of zinc speciation toward higher concentrations of ZnS is shown below 17 cm. This figure gives the major zinc species calculated concentration as percent total zinc as a function of depth as well as the total concentration of zinc. Note that although the total zinc

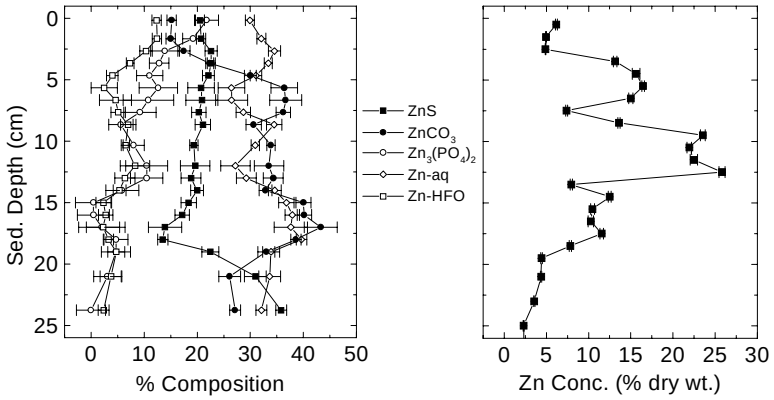

Figure 7.4: Zn speciation and concentration calculated as a function of depth at site C1. Vertical scales are the same for both graphs.

concentration for this site approached up to 30%, these concentrations are given as dry weight measurements. The EXAFS samples were examined in their natural, wet state, which is was composed of nearly 70% water. Thus, the EXAFS measurements were performed at zinc concentrations at maximum around 9%, which is at the upper limit of the acceptable range for fluorescence measurements, *i.e.* where self-absorption effects are minimal (Heald, 1988).

Site C1 shows a large proportion of hydrated zinc throughout the sampled core (25-40%) as well as a high concentration of carbonate species below 5 cm. Since the C1 site has high concentrations of total zinc in the sediments and the water column, the high fraction of hydrated zinc is not surprising. Hydrated zinc is the zinc that is indistinguishable from the aqueous ion by X-ray absorption experiments. This essentially means that it is the component of Zn that has only hexa-coordinate oxygen as a single backscattered peak. This category likely contains some soluble zinc, but is

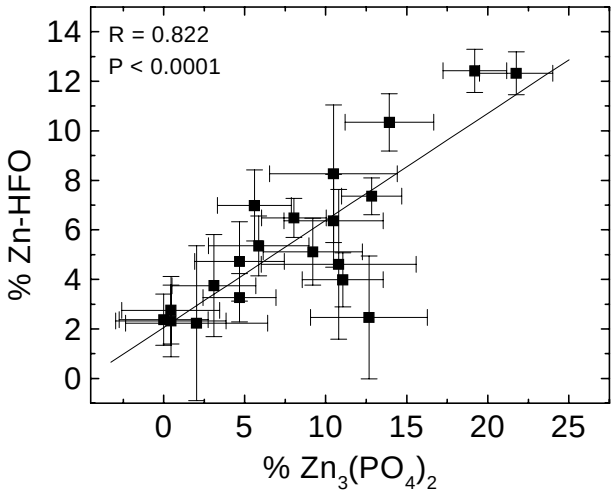

Figure 7.5: Plot of zinc phosphate vs. zinc associated with iron oxides for site C1. The strong correlation of these two components suggests that the phases are closely related.

mostly zinc loosely bound to surfaces, such as silicates or oxides. The concentration of aqueous zinc in the sediment (*c.a.* 200 μM) is not high enough to contribute to a significant portion of the EXAFS signal. Thus, the hydrated zinc found in the sediments must be a result of another species. Previous studies (Strawn and Sparks, 1999) have shown that metals bound in an outer-sphere complex show an EXAFS signature that is similar to the free, aqueous metal ion. EXAFS of zinc adsorbed onto iron oxides (chosen as one of the standards in the basis set) shows distinct backscattering atoms other than oxygen, which supports an inner-sphere complexation of zinc to the oxide surface. This supports the view in the literature that metals such as zinc are likely to form inner-sphere complexes with iron oxides (Brown *et. al.*, 1989; Stumm and Morgan, 1996). This implies that a large fraction of the zinc adsorbed to particles at this site have weak outer-

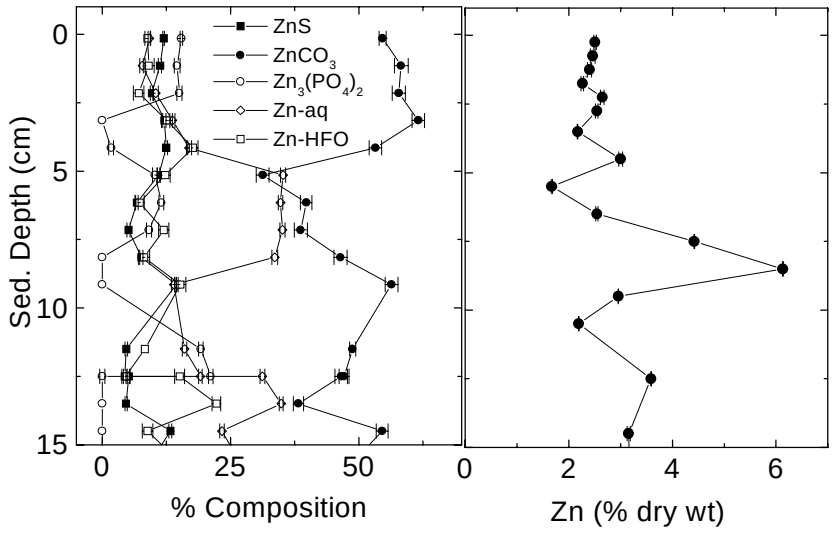

Figure 7.6: Zn speciation and concentration calculated as a function of depth at site C2. Vertical scales are the same for both graphs.

sphere complexation to silicates and other minerals, rather than iron oxides. This suggests that a large portion of the zinc at this site is relatively labile and easily transportable.

Additionally, the zinc tied up in iron oxides and phosphates trend together over most of the core and has a correlation coefficient of 0.822 as shown in Figure 7.5. The error bars on the compositions of these samples is rather large, but is unavoidable due to the fact that these two components are a relatively small proportion of the total zinc. However, the trend that results is still useful for qualitative interpretation.

Analytical electron microscopy (AEM) of these sediments (Webb *et. al.*, 2000) has shown that a significant fraction of the zinc containing colloidal matter present is composed of

iron-zinc-phosphates. The apparent spectral decomposition of the EXAFS signal however, calculates this category of particle as two separate components; zinc phosphate and zinc bound to iron oxide. A possible explanation for these colloids is that iron oxides which form as anoxic groundwater enter the creek (many groundwater seeps which are coated in ochre and orange iron oxides can be observed at the head of the creek), rapidly adsorb phosphate which is in relatively high concentrations at the site. This then leads to the precipitation of zinc phosphates on the surface of the iron oxides. However, the zinc present in the particles is at much higher concentrations than could be allowed for purely adsorption phenomena as determined by AEM. Solely surface bound zinc would not be detectable by these means. Additionally, this would lead to an EXAFS signature that should show significantly more Zn-PO_4 binding than Zn-oxide binding. The ratio of PO_4-HFO bound Zn found at this site, although slightly favoring

Zn-PO_4, is not large enough to support the above hypothesis. Thus, it is most likely that the colloidal iron-zinc-phosphates are formed as autochthonous particles in a coprecipiation event in the sediment or water column. This process of particle formation is also supported by the AEM cross sections that were discussed in Chapter 8.

Sediment EXAFS results from the deltaic site, C2, is shown in Figure 7.6. The most striking feature in the speciation of zinc at this location is the cyclical nature of $Zn_3(PO_4)_2$. The relative concentration of zinc phosphates oscillates between nearly absent to about 15% with a period of about 4-5 cm. This suggests a seasonal effect in the composition of

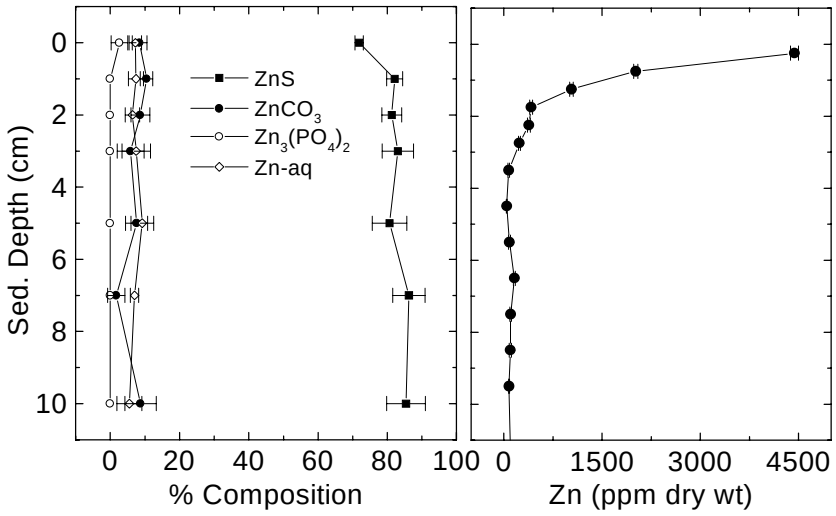

Figure 7.7: Zn speciation and concentration calculated as a function of depth at site M1. Vertical scales are the same for both graphs.

deposited sediments at this site. This is supported by the sedimentation rate measured in the lake previously at 3-4 cm yr^{-1} (Cahill and Steele, 1986). Since the lake is prone to flooding events, this may represent changes in the source material depending if the lake is at a low or high level. These phosphates are likely derived from site C1 upstream. The EXAFS speciation given in Figure 7.7 shows that the zinc at M1 is dominated almost entirely by ZnS. Additionally, there is much less hydrated zinc here than at the other sites. This is likely due to the fact that the site is removed from the bulk contamination and that the sediments are more consolidated and contain proportionately less water. These changes in the zinc composition can be interpreted from the geochemical processes that occur in the lake sediments at each site. In general, the presence of zinc carbonate phases in the upper sediments will occur due to increase in carbon dioxide as a result of the mineralization of organic matter. At depth, production of HS^- by

microbial mediated reduction of SO_4^{2-} begins to convert zinc to ZnS. Since the zinc concentrations are much larger than the sulfide produced, there is very little free sulfide in the upper layers of the sediment. This also allows the coexistence of less insoluable phases, such as carbonates, to be present along with the ZnS. As the metal concentrations decrease at the bottom of the C1 core sample, ZnS becomes of greater importance in terms of the dominant solid phases. In a location where the metal concentrations are very low, such as at M1, we see that the zinc speciation is dominated by sulfides throughout the core.

Additionally, interesting observations can be seen in the zinc speciation across the gradient in contamination at these sites. The amount of zinc present in the sediments and water column at each site decreases from site C1 to C2 to M1. At the highest concentrations of zinc, the speciation is dominated by forms that are extremely to relatively labile, *i.e.* hydrated zinc and carbonates respectively. As this is where the zinc has initially entered the lake system, we might expect to see the dominant form as a labile or readily transportable species.

This is in sharp contrast to the M1 site, where what little zinc present is the form of insoluble sulfides. Previous work (Rimstidt *et. al.*, 1994) has shown that ZnS oxidation is kinetically limited, so even if these sediments were resuspended, they may not lead to a significant release of metal contaminants. The fact that the M1 site is relatively close to the source of zinc to the lake also suggests that the overall lability of the zinc species drops rapidly upon entering the lake. Thus, although entering the lake, zinc appears to

be readily transportable but rapidly removed from the water column and deposited in the sediments. This removal explains the lack of significant zinc concentrations in the far reaches of the lake.

The C2 site shows a combination of these effects. On one hand, during part of the year the site is heavily inundated with lake water, and the sedimentation patterns follow that more of a mid-lake site. During the summer and early autumn, the lake levels drop and the surrounding area becomes wetland and marsh-like. In this period, the deposition of sediments will be dominated by the outflow of the stream. Thus, we see periods of deposition that contain proportionately more zinc phosphates.

7.2 COMPARISON TO SEQUENTIAL EXTRACTION RESULTS

Sequential extraction was used to compare the results of the XAS spectral deconvolution to traditional wet chemical methods. These extractions aim to selectively extract metals from specified phases depending on the chemical extractant. Common phases that can be extracted are ion-exchangeable sites, carbonates, iron and manganese oxides, and organic matter. The remaining metals not extracted from the previous phases are termed “recalcitrant” or “residual” metals. These can include various metal oxides and silicate metals. Metals that are tightly bound in silicate matrices are not extracted in this procedure, since it normally requires concentrated hydrofluoric acid to dissolve these phases.

Table 7.1 shows the results of the sequential extraction on sediments retrieved near the C2 site at Lake DePue. These samples were performed on cores extracted from the lake in August of 2000. Extractions and EXAFS deconvolution were performed on a single core from the C2 site. The extractions show that most of the zinc present dissolves in the acetate extractions step, which targets carbonated species, and the hydroxylamine step, which targets iron and manganese oxides. Smaller amounts of zinc are present in the ion-exchangeable, organic matter, and residual fractions. Sediments taken from the upper 5 cm of this site all showed the same general proportions between the phases as determined by sequential extraction. The EXAFS determination of the same sediment is also presented in Table 7.1. Note that this sediment was collected in a different year and at a different season than the core profiles of C2 shown in Figure 7.6. The difference in the EXAFS calculations of zinc speciation between years illustrates the high degree of spatial and temporal variations that exist in the sediments of Lake DePue.

Table 7.1: Comparison between calculated zinc speciation using EXAFS spectral deconvolution and sequential extraction. All phases are reported in percent of the total zinc in the sample.

EXAFS		Sequential Extraction	
Zn-aq	8.6% ± 2.8	Ion Exchangeable	5.6% ± 1.2
$ZnCO_3$	36.7% ± 5.2	Carbonate	40.6% ± 2.3
$Zn_3(PO_4)_2$	43.0% ± 4.5	Iron Oxide	42.3% ± 1.7
Zn-FeOx	4.5% ± 2.1		
		Organic	4.6% ± 2.1
ZnS	7.1% ± 1.4	Residual	6.8% ± 3.0

The EXAFS calculations of the sediment agree reasonably well with the sequential extraction results on most of the targeted phases, with the exception of the iron oxides. For example, the aqueous zinc phase determined by EXAFS closely matches the ion exchangeable fraction from the chemical extractions. The percentage of carbonates determined by these two methods also agrees very well within the degree of error for the two techniques. If we assume that the sulfidic phases will not extract until treated to acidic environments, then the zinc sulfide phases in the EXAFS fit also matches well with the residual fraction in the extractions. Unfortunately, the basis set used for the EXAFS spectral deconvolutions did include an analogue for zinc bound with organic matter. This would be a difficult standard to construct, as the quality of organic matter is variable between different field sites. Future expansions of the basis set could include zinc bound to model humic and fulvic acids for this fraction. A distinct limitation for EXAFS determinations of heavy metals may be that it is only useful in field settings where the metal of interest is not bound to a significant degree to organic matter. Since the sequential extraction shows that only 4% of the zinc is associated with organic matter, it is unlikely that it adversely affects present EXAFS spectral decompositions.

The main discrepancy that is left in pairing the two results is the hydroxylamine fraction. The sequential extraction results give that about 42% of the zinc in the sediment is extracted in this step. However, the EXAFS fitting only accounts for at most 5 or 6% of the zinc as those bound in iron oxides. The disagreement is likely to result from the amounts of phosphates that are found in the sediment. Both EXAFS and AEM found that phosphate phases were important in the speciation of zinc. The extraction

procedure described above does not target specifically a phosphate phase. Initially, the zinc phosphates may be expected to extract in the same step as the carbonates, *i.e.*, in a mildly acidic environment. However, the AEM results from Chapter 8 also suggested that iron was also an important co-cation in the zinc-phosphate colloids found in the sediments. With this realization, it is possible that the phosphates in the sediment is closely tied in iron complexes and in turn do not dissolve until the iron oxide matrix is attacked by the hydroxylamine extraction step. If we take this approach and sum the zinc phosphate and zinc-iron oxide phases from the EXAFS determination, we see that the result closely matches the amount of zinc extracted in the hydroxylamine step.

Although these first comparisons are very encouraging, further work with parallel EXAFS determination and sequential extractions needs to be performed in order to more accurately validate the EXAFS procedure for sediment speciation. In particular, a "standard addition" type procedure, where a known phase is added in increasing amounts to a sediment sample should be performed to determine if both procedures see the increases in the same fractions. Also, more work to compare the EXAFS of various zinc-iron phosphates is also required to determine if this is a necessary component to include in the basis set of standards for future determinations.

Even with the need for further work, this study shows the usefulness in determining the speciation of zinc in a contaminated system using X-ray spectroscopy. The initial attempt at validating the XAS technique with traditional sequential extractions shows that the two agree in most of the calculated fractions. The main advantage of this

procedure comes from the fact that measurements are performed non-destructively. Additionally, when used with complementary techniques such as AEM, one can have an independent verification of analytical results obtained on both the bulk scale and on the individual particle scale.